Integral Force/Moment Waterjet Model for CFD Simulations

Manivannan Kandasamy

Seng Keat Ooi

Pablo Carrica

Frederick Stern[1]
e-mail: frederick-stern@uiowa.edu

IIHR-Hydroscience and Engineering,
The University of Iowa,
Iowa City, IA 52242

An integral force/moment waterjet model for computational fluid dynamics (CFD) is derived for ship local flow/powering predictions, including sinkage and trim. The waterjet induced reaction forces and moment and waterjet/hull interaction stern force replicate the effects of the waterjet without requiring detailed simulations of the waterjet system. The model extends the International Towing Tank Conference (ITTC) waterjet model for sinkage and trim by using an alternative control volume also appropriate for CFD and by including vertical forces and pitching moment in the waterjet/hull force/moment balance. The same grid is used for both without and with waterjet simulations. The CFD waterjet model requires limited waterjet geometry (inlet and outlet areas and locations, and weight of working fluid) and several waterjet flow (mass flow rate, inlet pressure force, inlet and outlet momentum correction factors and flow angles, and stern force and location) input variables. The CFD waterjet model can be used for local flow predictions by using waterjet flow input variables provided by ITTC waterjet model test data, including additional data for waterjet induced inlet pressure and stern forces. It can also be used for powering predictions once waterjet flow input variable correlations are available based on CFD for the waterjet system and/or experimental data. The CFD waterjet model is demonstrated for local flow predictions for the DTMB 5594 high-speed sealift ship model for which ITTC waterjet model test data, including additional data for waterjet induced stern forces, are available. Correlations for the waterjet flow input variables are shown to be feasible using a combination of CFD and experimental data for the waterjet system for three different hulls. [DOI: 10.1115/1.4002573]

1 Introduction

Waterjet (WJ) propulsion systems are increasingly being used for high-speed ships. Most CFD is for the waterjet system alone without considering waterjet/hull interaction or powering prediction due to the difficulty of geometry modeling and grid generation for the combined ship and waterjet systems, as reviewed by the report of the 24th ITTC Specialized Committee on Validation of Waterjet Test Procedures [1]. Stern et al. [2] demonstrated CFD capability for simulating waterjet self-propelled high-speed trimaran sealift ships including above water discharge in both calm water and irregular head waves at sea state 6 conditions using CFDSHIP-IOWA [3]. Kandasamy et al. [4] carried out a detailed validation of the waterjet performance predictions for the joint high-speed sealift (JHSS). However, for some applications, details of the waterjet induced flow are not required, and a simplified force/moment waterjet model is desirable, conceptually similar to that developed previously for propeller propulsion systems [5]. The present study was motivated by the need to model the waterjet's effect on the trim of high-speed, low-wake, and semiplanning passenger ferries cost effectively during the initial design stages, as the trim affects both the resistance and wake height significantly [6].

The ITTC [1] has developed waterjet test procedures, which combine model testing with control volume/integral analysis for ship powering predictions hereafter referred to as the ITTC waterjet model. Herein, an integral force/moment waterjet model for CFD is derived for ship local flow/powering predictions, including sinkage and trim. The waterjet induced reaction forces and moment and waterjet/hull interaction stern forces replicate the effects of the waterjet without requiring detailed simulations of the waterjet system. The model extends the ITTC waterjet model for sinkage and trim by using an alternative control volume also appropriate for CFD and by including vertical forces and pitching moment in the waterjet/hull force/moment balance. The same grid is used for both without and with waterjet simulations. The CFD waterjet model requires limited waterjet geometry (inlet and outlet areas and locations, and weight of working fluid) and several waterjet flow (mass flow rate, inlet pressure force, inlet and outlet momentum correction factors and flow angles, and stern force and location) input variables. The CFD waterjet model can be used for local flow and sinkage and trim predictions by using waterjet flow input variables provided by ITTC waterjet model test data, including additional data for waterjet induced inlet pressure and stern forces. It can also be used for powering predictions once waterjet flow input variable correlations are available based on CFD for the waterjet system and/or experimental data. The CFD waterjet model is demonstrated for local flow predictions for the DTMB 5594 high-speed sealift ship model for which ITTC waterjet model test data, including additional data for waterjet induced stern forces, are available. Correlations for the waterjet flow input variables are shown to be feasible using CFD for the waterjet system for three different hulls.

2 ITTC Waterjet Model

The ITTC waterjet model combines model testing with control volume/integral analysis for ship powering predictions. Such procedures are required due to difficulties for a direct measurement of the waterjet net thrust.

The ITTC waterjet model control volume set in the carriage-fixed inertial frame of reference, shown in Fig. 1, was selected for the waterjet system in order to be able to compute or determine the powering characteristics from measurements, considering (1) the ease of measurement of momentum and energy fluxes across the inlet and outlet, (2) that control volume boundaries capture all inflow and outflow of the waterjet system, and (3) that the protruding part of the control volume defined by surface ABC should be as small as possible to avoid strong interaction effects with the external flow. The selected control volume is defined by a stream-

[1]Corresponding author.

Contributed by the Fluids Engineering Division of ASME for publication in the JOURNAL OF FLUIDS ENGINEERING. Manuscript received February 2, 2008; final manuscript received August 25, 2010; published online October 20, 2010. Assoc. Editor: Joseph Katz.

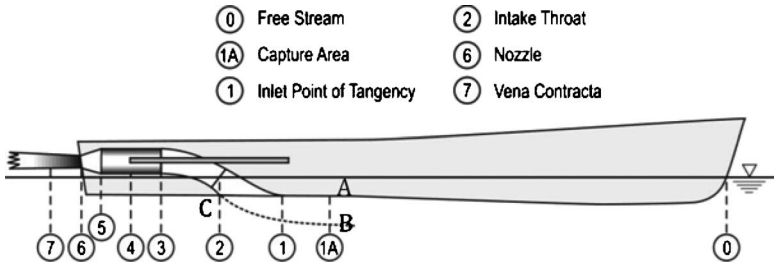

Fig. 1 ITTC waterjet model control volume

tube consisting of the nozzle, pump, ducting system, inlet, and upstream imaginary surface BC in the flow through which it is assumed that no mass transport occurs by definition with one outlet A_6 and inlet A_{1A}. Vertical reaction force, weight of the working fluid, and pressure and shear forces acting on BC are neglected. The inlet A_{1A} is selected to avoid major flow distortions by the intake geometry and as practical choice is usually one impeller diameter in front of the ramp tangency point.

The ITTC model procedures provide a series of standardized tests for the prediction of the main powering characteristics such as power-speed and impeller rotation rate–speed relations. The procedures are presented in global terms, leaving sufficient freedom for individual institutes to use their own preferred methods. The first step is the collection of data such as nozzle area, A_6, hull length L_{pp}, and static wetted surface area A_S.

The second step is the resistance test and wake-field measurements where a resistance test is carried out for a bare hull model with closed intakes that is free to sink and trim. The total bare hull resistance R_{TBH} is obtained and is used later to estimate the thrust deduction factor, t. During the resistance test, the boundary layer velocity profile $u_{1AX}(y,z)$ is measured at Station 1A. This profile will be used later to calculate the following items: the intake area at Station 1A, the average velocity at Station 1A, $\bar{V}_{1A}$, and the momentum correction factor at Station 1A, c_{m1}, which is calculated at any Station N using

$$c_{MN} = \frac{1}{A_N}\int_{A_N}\left(\frac{u}{\bar{V}_N}\right)^2 dA \tag{1}$$

$$\bar{V}_N = \frac{1}{A_N}\int_{A_N}(V\cdot n)dA \tag{2}$$

The third step is the calibration and propulsion tests. The purpose of the calibration test is to establish a relation between a measurement signal at the jet (often, a differential pressure transducer or Kiel probe is used) and the jet thrust (T_{Jx}), which is measured through the Bollard pull test. The flow rate (Q) is then calibrated through the momentum flux approach since a direct measurement of the flow rate is prone to higher uncertainties. Assuming a negligible inlet axial velocity, T_{Jx} is equal to the momentum flux at the jet nozzle, providing Eq. (3) for estimating Q,

$$Q = \sqrt{\frac{T_{Jx}A_6}{\rho c_{m6}\cos\alpha}} \tag{3}$$

During the calibration phase, the momentum correction factor at the jet exit c_{m6} is obtained from detailed jet velocity profiles using laser Doppler velocimetry (LDV). α is the jet angle relative to the horizontal at the nozzle (Station 6). This calibration is assumed to hold good even with nonzero forward velocity, so that the Kiel probe measurements taken during self-propulsion tests could be used to estimate Q.

After calibration, the propulsion test is carried out to determine the relation between speed, flow rate, and thrust at the self-propulsion point. Note that the ITTC model procedure recommends that the self-propulsion point be determined through thrust identity, which requires that the nondimensional thrust loading be the same in both full and model scales. The model must then be towed with a make-up added tow force to account for the higher friction in the model scale due to the thicker boundary layer, which is defined as

$$F_D = \tfrac{1}{2}\rho U_0^2 S(C_{Fm} - C_{Fs}) \tag{4}$$

where U_0 is the desired model velocity, S is the model wetted surface area, and C_{Fm} and C_{Fs} are the model and ship friction coefficients, calculated from the ITTC ship-model correlation.

The calibrated Kiel probe measurements provide Q at the self-propulsion point. Q is then used to determine the size of the inlet capture area from the inlet wake-field measurements by applying conservation of mass. Once the capture area is determined, c_{m1} can be calculated. All the relevant variables to predict the waterjet net thrust (R_X) from Eq. (5) are now known,

$$-R_X = \frac{\rho Q^2}{A_6}c_{M6}\cos\alpha - \rho Q c_{M\mathrm{in}}U_0 \tag{5}$$

which can alternatively be written as in

$$R_X = -\dot{m}(c_{M6}\bar{V}_{6X}\cos\alpha - c_{M\mathrm{in}}\bar{V}_{\mathrm{in}X}) \tag{6}$$

Notice that the ITTC model ignores vertical forces and pitching moments needed to evaluate sinkage and trim in a CFD simulation. These are not relevant for the purposes of the original ITTC model since sinkage and trim are measured during the thrust evaluation procedure. For a CFD simulation, however, it is desirable to estimate the resulting waterjet induced forces and moments affecting sinkage and trim since the final attitude of the ship affects the resistance and wave-generation characteristics of the ship.

3 CFD Waterjet Model

The purpose of the CFD waterjet model is for ship local flow/powering predictions including sinkage and trim without requiring detailed simulations for the waterjet system (nozzle, pump, ducting system, and inlet). The control volume shown in Fig. 2 is selected with consideration to (1) implementation simplicity in CFD using the same grid as for without waterjet simulations by representing the waterjet system by axial and vertical reaction forces and pitching reaction moment, and by representing the waterjet/hull interaction using a vertical stern force, (2) ability to

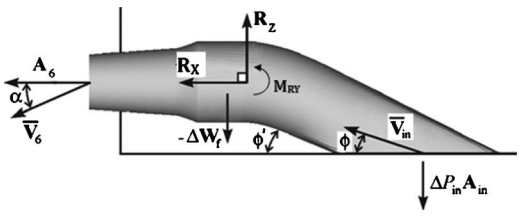

Fig. 2 CFD waterjet model control volume

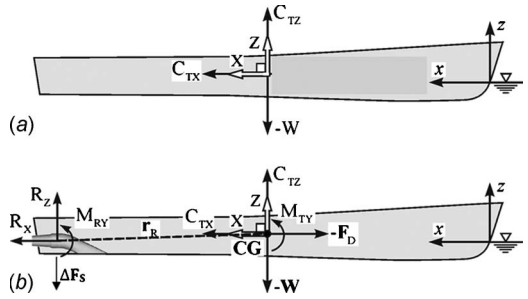

Fig. 3 Forces and moments on a towed ship model: (*a*) bare hull simulation and (*b*) waterjet-propelled simulation

predict either speed for given powering or vice versa including sinkage and trim, and (3) require as limited number of empirical correlations as possible. The selected control volume is similar to the ITTC model, except the imaginary surface BC in the flow is removed and the inlet is taken as the actual inlet to the waterjet across the bottom plane of the hull. The flow angles with respect to the keel at the intake and nozzle are ϕ and α, respectively. The waterjet induced forces on the control volume are $\Delta P_{\text{in}}\mathbf{A}_{\text{in}}$, the change in pressure force on the hull at the location of the intake, and $\Delta\mathbf{W}_{\mathbf{f}}$, the weight of water in the waterjet dead volume. The waterjet induced pressure at the outlet is usually small, therefore not included, but can be easily incorporated.

The choice of the proposed control volume for the waterjet instead of the ITTC control volume is also motivated by the possibility of experimentally measuring the pressure and velocities at the waterjet inlet, which allows for the computation of the inlet flow angle ϕ, momentum flux correction factor $C_{M\text{in}}$, pressure force $\Delta P_{\text{in}}\mathbf{A}_{\text{in}}$, and pressure distribution at stern, which provides the waterjet/hull interaction stern force $\Delta\mathbf{F}_{\text{S}}$. The ITTC control volume is limited by a streamtube entering the waterjet duct, determining the limiting streamlines forming the streamtube and measuring pressures on its surface for the purposes of calculating vertical forces and pitching moments would be extremely difficult. Also, curved streamlines near the waterjet inlet point to strong pressure gradients, an additional indication that neglecting those pressure forces would be questionable.

Figure 3 shows the coordinate systems, forces, and moments for towed bare hull (Fig. 3(*a*)) and towed waterjet-propelled (Fig. 3(*b*)) ship models in a ship-fixed reference frame, which uses (X,Y,Z) coordinates, moving with constant velocity $(-U_0,0,0)$ in the relative inertial frame. The model ship is assumed free to sink and trim. The origin is located at the center of gravity CG $=(x_{\text{CG}},y_{\text{CG}},z_{\text{CG}})$, with the CG coordinates expressed in the usual absolute inertial CFD system (x,y,z) with $x=0$ located at the forward perpendicular of the ship at the rest condition in calm water with x positive downstream and $z=0$ at the calm water plane with z positive upward and the y coordinate pointing to starboard, forming a right hand system. The area shaded in gray in Fig. 3(*b*) shows the control volume for the waterjet model in the self-propelled ship. For convenience, the control volume analysis for the waterjet-propelled case uses Cartesian coordinates similar to (X,Y,Z), but with origin at the thrust bearing and position vector $\mathbf{r}_{\text{R}}$ relative to the CG, as shown in Fig. 3. The thrust bearing defined by a vector $\mathbf{r}_R$ from the CG (see Fig. 3(*b*)) is not necessary for the derivation of the waterjet model but is used because it makes the model conceptually easier to derive. Position vectors are defined from the thrust bearing to the intake $\mathbf{r}_{\text{in}}$, to the nozzle $\mathbf{r}_6$, and to the centroid of the weight of the fluid in the waterjet $\mathbf{r}_{\Delta Wf}$.

3.1 Integral Waterjet Force/Moment Analysis. The reaction forces and moment M_{RY} about the thrust bearing are obtained using the Reynolds transport theorem with the ship-fixed, nondeforming control volume for steady, incompressible flow.

At the inlet,

$$\overline{\mathbf{V}}_{\text{in}} = \overline{V}_{\text{in}}\cos\phi\mathbf{i} + \overline{V}_{\text{in}}\sin\phi\mathbf{k} = \overline{V}_{\text{in}X}\mathbf{i} + \overline{V}_{\text{in}Z}\mathbf{k} \tag{7}$$

and at the outlet,

$$\overline{\mathbf{V}}_6 = \overline{V}_6\cos\alpha\mathbf{i} + \overline{V}_6\sin\alpha\mathbf{k} = \overline{V}_{6X}\mathbf{i} + \overline{V}_{6Z}\mathbf{k} \tag{8}$$

The conservation of linear momentum gives the reaction force,

$$-\mathbf{R} = \dot{m}(c_{M6}\overline{\mathbf{V}}_6 - c_{M\text{in}}\overline{\mathbf{V}}_{\text{in}}) - \Delta P_{\text{in}}\mathbf{A}_{\text{in}} + \Delta\mathbf{W}_f \tag{9}$$

Equation (9) is decomposed into axial and vertical components as follows:

$$R_X = -\dot{m}(c_{M6}\overline{V}_{6X} - c_{M\text{in}x}\overline{V}_{\text{in}X}) + \Delta P_{\text{in}}A_{\text{in}X} - \Delta W_{fX} \tag{10}$$

$$R_Z = -\dot{m}(c_{M6}\overline{V}_{6Z} - c_{M\text{in}z}\overline{V}_{\text{in}Z}) + \Delta P_{\text{in}}A_{\text{in}Z} - \Delta W_{fZ} \tag{11}$$

Equation (10) reduces to Eq. (6) if $\Delta P_{\text{in}}A_{\text{in}X}$ can be neglected and $\Delta W_{fX}=0$. Note that the sign of the $\Delta P_{\text{in}}A_{\text{in}X}$ term may change depending on the orientation of vector $\mathbf{A}_{\text{in}}$.

The conservation of angular momentum gives reaction pitching moment about the thrust bearing M_{RY},

$$M_{RY} = (-\dot{m}(\mathbf{r}_6\times c_{M6}\mathbf{V}_6 - \mathbf{r}_{\text{in}}\times c_{M\text{in}}\mathbf{V}_{\text{in}}) + (\mathbf{r}_{\text{in}}\times\Delta P_{\text{in}}\mathbf{A}_{\text{in}}) + (\mathbf{r}_{\Delta Wf} \times \Delta\mathbf{W}_f))\cdot\mathbf{j} \tag{12}$$

3.2 Waterjet/Hull Force/Moment Balance. The force and moment of the waterjet system on the ship is obtained from the equilibrium of forces and moments on the ship using the ship-fixed (X,Y,Z) coordinate system, as shown in Figs. 3(*a*) and 3(*b*) without and with waterjet conditions, respectively. CFD simulations provide the hydrodynamic forces $\mathbf{C}_T=(C_{TX},0,C_{TZ})$ and moment M_{TY} transformed into the (X,Y,Z) coordinate system.

The equilibrium of forces and moments for the waterjet-propelled condition requires that

$$\sum F_X = C_{TX} + R_X + \Delta F_{SX} - F_D\cos\tau - W\sin\tau = 0 \tag{13}$$

$$\sum F_Z = C_{TZ} + R_Z + \Delta F_{SZ} - W\cos\tau - F_D\sin\tau = 0 \tag{14}$$

$$\sum M_Y = M_{RY} + (\mathbf{r}_R\times\mathbf{R})\cdot\mathbf{j} + (\mathbf{r}_{\Delta FS}\times\Delta\mathbf{F}_S)\cdot\mathbf{j} + M_{TY} = 0 \tag{15}$$

F_D is the added tow force in the axial direction of the carriage, W is the weight of the ship, $\mathbf{r}_{\Delta FS}=(X_{FS},0,Z_{FS})$ is the position vector from the CG to $\Delta\mathbf{F}_{\text{S}}$, and τ is the trim angle. Expanding Eq. (15) results in

$$\sum M_Y = M_{\text{WJ}} + M_{TY} = 0 \tag{16}$$

where

$$M_{\text{WJ}} = M_{RY} + Z_R(R_X) - X_R(R_Z) + Z_{FS}(F_{SX}) - X_{FS}(F_{SZ}) \tag{17}$$

Equations (13)–(17) can also be used for the towed bare hull simulations by setting all the waterjet forces R_X, R_Z, F_{SX}, F_{SZ}, moments M_{RY}, M_{WJ}, and position vectors $\mathbf{r}_{\Delta FS}$, $\mathbf{r}_R$ in the equations to zero.

In summary, the CFD waterjet model includes vertical reaction force, weight of the working fluid, pressure forces acting on the inlet, and pitching moments. Additionally, the waterjet/hull interaction is represented by a waterjet induced stern force, which is included in the waterjet/hull force/moment balance. The input variables required are for geometry, $\mathbf{A}_{\text{in}}$, $\mathbf{A}_6$, $\mathbf{r}_R$, $\mathbf{r}_{\text{in}}$, $\mathbf{r}_6$, $\mathbf{r}_{\Delta Wf}$, and $\Delta\mathbf{W}_{\mathbf{f}}$, and for waterjet flow, $\dot{m}$, $\Delta P_{\text{in}}\mathbf{A}_{\text{in}}$, $c_{M\text{in}}$, c_{M6}, ϕ, α, and $\Delta\mathbf{F}_{\text{S}}$. For the present validation of the waterjet model, these input variables are acquired from experiments on DTMB 5594. The feasibility of acquiring these input variables from correlations is discussed in Sec. 6.

Table 1 Errors in % data from previous CFD simulations using CFDSHIP-IOWA

	Resistance	Sinkage	Trim
5512 [7]	4.3	7.4	10.4
Towed Athena [8]	2.1	7.7	9.6
Propelled Athena [8]	4.5	8.1	5.0
HSSL-Delft catamaran [2]	8.0	23.0	17.0

4 Computational Method

The waterjet model was implemented in CFDSHIP-IOWA version 4.0. CFDSHIP-IOWA version 4.0 [3] makes use of a single-phase level set method, advanced iterative solvers, conservative formulations, and a dynamic overset grid approach for simulating 6DOF ship motions in free surface viscous flows. The code has been validated for various cases, the most relevant of which are for DTMB 5512 pitch and heave [7], high-speed towed and self-propelled simulations of R/V Athena [8], and high-speed (Fr >0.4) sealift ships in various conditions [2]. The results are summarized in Table 1.

The fluid and the rigid multibody systems of equations can be solved either in an absolute inertial system (the earth system) or in a relative inertial system moving at the constant ship forward speed (the towing tank carriage system). This allows the use of several moving ships and, within each ship, the use of rotating propellers and rudders. For the present case, a relative inertial system was used where the forces and moments are computed on the relative inertial system and then projected into the local non-inertial system of coordinates, i.e., the ship-fixed reference frame, to solve the rigid-body equations and obtain the motions. Once the new positions of the moving objects are known, the grids are displaced and the grid point velocities are used as boundary conditions for the nonslip surfaces.

The computational domains extend from $-0.5<x<2$, $0<y<1$, and $-1<z<0.25$ in dimensionless coordinates based on L. Boundary conditions are shown in Table 2. Taking advantage of the problem symmetry, a half-domain overset grid, as shown in Fig. 4, was used with 1.4×10^6 grid points for the body-fitted ship grid and 400,000 grid points for the Cartesian background grid.

Table 2 Boundary conditions

Boundary conditions	Description
Inlet	$(U,V,W)=(1,0,0)$, $\partial P/\partial x=0$
Exit	$\partial^2(U,V,W)/\partial x^2=0$, $\partial P/\partial x=0$
No-slip	$(U,V,W)=0$, $\partial P/\partial n=0$ (where n is normal to the boundary)
Symmetry	$\partial(U,W,P)/\partial z=0$, $V=0$
Far-field 1	$\partial(U,V,W)/\partial n=0$, $\partial P/\partial n=0$
Far-field 2	$\partial(U,V,W)/\partial n=0$, $P=0$
At free-surface interface	$\partial(U,V,W)/\partial n=0$, $p=\frac{z}{\mathrm{Fr}^2}$

The grid design and number of points were deemed adequate for the present purpose based on previous verification studies for similar geometry and conditions. Computational grids for the hull were designed to accurately resolve geometric features of the model and the unsteady turbulent boundary layer, wake, and wave fields. The grids were generated using GRIDGEN. The hull boundary layer has a double-O topology and was created with a hyperbolic grid generator, with a grid spacing at the hull designed to yield $y^+<1$. This grid was free to move with the ship.

Three to five inner iterations were used for the convergence of the flow field equations within each time step. Convergence of the pressure equation is reached when the residual imbalance of the Poisson equation drops six orders of magnitude. All other variables are assumed converged when the residuals drop to 10^{-5}.

5 Demonstration and Validation of WJ Model for 5594

The CFD waterjet model was demonstrated and validated with simulations for the DTMB 5594 high-speed sealift ship model for which waterjet geometry and most flow input variables are available from experiments [9]. The validation data are for Fr $=U_0/\sqrt{gL_0}=0.511$ and $\mathrm{Re}=U_0L_0/\nu=2.9\times10^7$. Global and local flow measurements were made for bare hull resistance and self-propelled conditions. The net waterjet thrust was estimated using the ITTC waterjet recommended procedures and guidelines. Local flow measurements include axial velocity contours upstream of

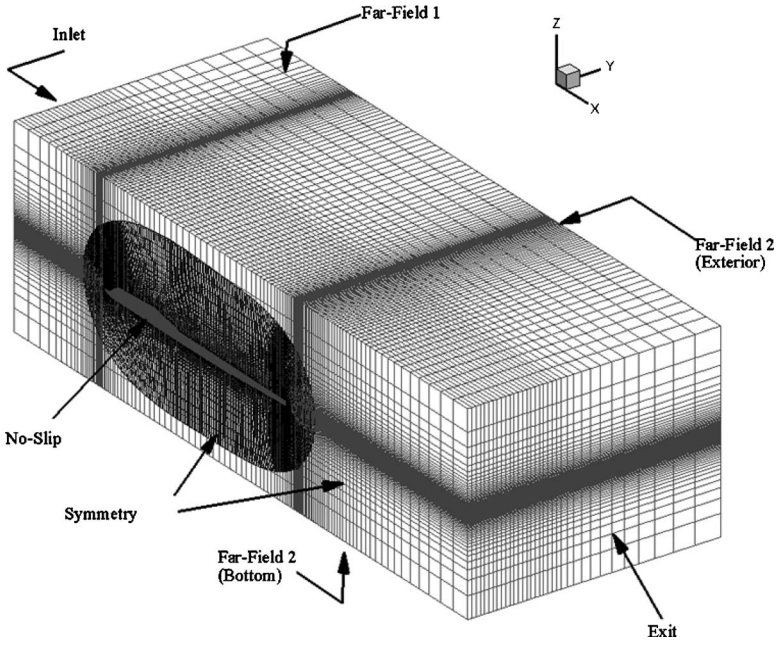

Fig. 4 Overset grid design and boundary conditions

the inlet, surface pressure distribution over the stern downstream, between, and upstream of the inlet both without and with waterjet conditions, and all required ITTC waterjet input variables.

For validation purposes, in consideration of the available experimental fluid dynamics (EFD) benchmark data, the CFD waterjet model was implemented with towed propelled conditions, i.e., with prescribed speed and waterjet induced vertical reaction force and moment. The resistance, sinkage, and trim were predicted. Since the ship model is at the self-propulsion point, the difference between EFD R_X, sinkage, and trim and CFD C_{TX}, sinkage, and trim provides an assessment of the capability of the CFD waterjet model. Simulations and comparisons with EFD are also done for the bare hull condition, thereby providing an assessment of the prediction of waterjet induced changes.

5.1 Evaluation of CFD Waterjet Model Input Variables for 5594. Wilson et al. [9] provided the waterjet flow variables R_X, $\dot{m}$, c_{M6}, and $\Delta\mathbf{F}_S$ and most of the geometries $\mathbf{A}_{\text{in}}$, $\mathbf{A}_6$, $\mathbf{r}_R$, $\mathbf{r}_{in}$, and $\mathbf{r}_6$. α was assumed zero, as per the waterjet geometry. Detailed surface grid information and preliminary CFD solutions for the same geometry and conditions, including waterjet system, provided $\mathbf{r}_{\Delta Wf}$, $\Delta\mathbf{W_f}$, and $c_{M\text{in}}$ [10]. The required input parameter ϕ was unavailable. Hence, R_X was used to estimate ϕ by control volume analysis as follows.

Since $\alpha=0$, $\bar{V}_{6Z}=0$ and applying conservation of mass at exit gives

$$\bar{V}_{6X}=\frac{\dot{m}}{\rho A_6}=1.47U_0 \tag{18}$$

Solving Eq. (10) gives $\bar{V}_{inX}=0.730U_0$. Applying conservation of mass at the horizontal inlet gives

$$\bar{V}_{inZ}=\frac{\dot{m}}{\rho A_{inZ}}=0.216U_0 \tag{19}$$

The angle ϕ is obtained from

$$\phi=\tan^{-1}\left(\frac{\bar{V}_{\text{in}Z}}{\bar{V}_{\text{in}X}}\right)=16.45 \text{ deg} \tag{20}$$

which is shallower than the geometrical angle of the waterjet inlet $\phi'=27$ deg. If the geometrical angle $\phi'=27$ deg was used as an approximation for the inflow angle ϕ, the resulting R_X would be 7% larger than EFD.

Detailed pressure measurements were taken by Wilson et al. [9] on the stern of the model. The measurements were made across the width and length of the stern and in both directions included points surrounding the intakes but not in the intake itself. It was decided to estimate the pressure at the intake from the closest measurement points and the distributions of pressure measurements surrounding the intake. The detailed measurements were provided as nondimensional pressure coefficients C_P measured longitudinally along the centerline of the hull and the port side of the hull for both active and inactive waterjet conditions,

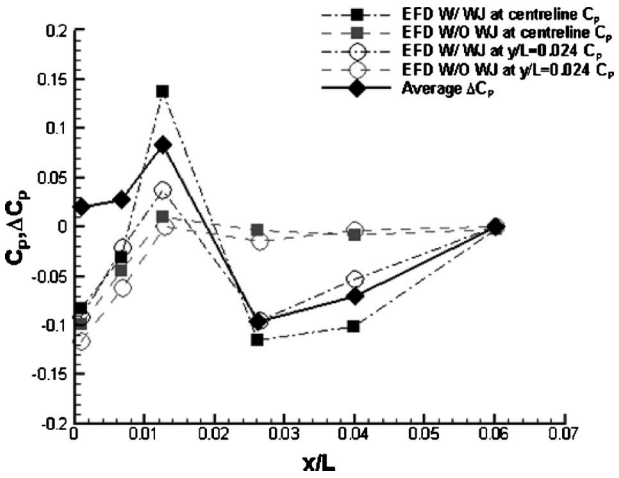

Fig. 5 C_P on the model afterbody

$$C_P=\frac{P-P_\infty}{\rho U_o^2} \tag{21}$$

The difference in C_P between active and inactive waterjet conditions at the centerline of the hull and the port side of the hull was then averaged to get the longitudinal distribution of ΔC_P along the stern (Fig. 5). This longitudinal distribution is assumed to hold over the total stern area A_{TZ}. The total stern force ΔF_{TZ} is obtained as

$$\Delta F_{TZ}=\Delta F_{SZ}+\Delta P_{\text{in}}A_{\text{in}Z}=\int_{A_{TZ}}\int \Delta C_P da \tag{22}$$

Table 3 summarizes the nondimensional CFD waterjet model input variables for the current implementation, and values used to nondimensionalize the input variables are tabulated in Table 4.

The CFD waterjet model reaction forces/moments and their components are summarized in Table 5. Based on the current assumptions/implementation the axial reaction force $R_X=-8.767\times10^{-5}$. The waterjet induced stern force ΔF_{TZ} is negative and more than twice as large as the vertical momentum flux M_Z,

$$M_Z=\dot{m}c_{M\text{in}Z}\bar{V}_{\text{in}Z} \tag{23}$$

The overall waterjet induced vertical force is negative and is equal to -3.6×10^{-5}. The waterjet induced pitching moment about the CG is positive, i.e., positive trim predominantly due to the moment of ΔF_{TZ} and small contribution from the moment of R_X.

5.2 Validation of Global Variables. Simulations were conducted for both towed bare hull and towed propelled conditions, and the resistance, sinkage, and trim were predicted. The error in the predicted total resistance (C_{TX}) for the towed bare hull simulation (Table 6) is $E=0.78\%$, where the relative error E is defined

Table 3 Data for CFD waterjet model for 5594

Geometry variables	Flow variables
$\mathbf{A}_{\text{in}}=\mathbf{A}^*_{\text{in}}/L_0^2=(0,0,5.60\times10^{-4})$	$\dot{m}=\rho Q/\rho U_0 L_0^2=1.207\times10^{-4}$
$\mathbf{A}_6=\mathbf{A}^*_6/L_0^2=(8.21\times10^{-5},0,0)$	$\Delta\mathbf{F}_S+\Delta P_{in}\mathbf{A}_{in}=(0,0,-6.35\times10^{-5})$
$\mathbf{r}_R=\mathbf{r}^*_R/L_0=(4.837\times10^{-1},0,-3.994\times10^{-3})$	$\Delta\mathbf{W}_f=(0,0,-6.213\times10^{-7})$
$\mathbf{r}_{\text{in}}=\mathbf{r}^*_{\text{in}}/L_0=(-1.997\times10^{-2},0,-6.753\times10^{-3})$	$\alpha=0^\circ$, $R_X=R^*_X/\rho U_0^2 L_0^2=8.767\times10^{-5}$
$\mathbf{r}_6=\mathbf{r}^*_6/L_0=(3.994\times10^{-3},0,0)$	$c_{Min\,X}=1.0594$, $c_{Min\,Z}=1.06$, $c_{M6}=1.019$
$\mathbf{r}_{\Delta FS}=\mathbf{r}^*_{\Delta FS}/L_0=(4.57\times10^{-1},0,-1.01\times10^{-2})$	$\bar{\mathbf{V}}_{in}=\bar{\mathbf{V}}^*_{in}/U_0=(0.730,0,0.216)$
$\mathbf{r}_{\Delta Wf}=\mathbf{r}^*_{\Delta Wf}/L_0=(1.005\times10^{-3},0,2.744\times10^{-3})$	$\bar{\mathbf{V}}_6=\bar{\mathbf{V}}^*_6/U_0=(1.47,0,0)$

Table 4 Model parameters for DTMB model for 5594

Density, r	1000 kg/m^3
Kinematic viscosity, n	1×10^{-6} m^2/s
Waterline length, L_0	6.956 m
Design speed, U_0	4.218 m/s
Froude number, Fr	0.511
Static wetted area, A_S	3.722 m^2
Water plane area, A_{WP}	2.463 m^2
Longitudinal moment of inertia, I_L	6.239 m^4

Table 5 Waterjet induced forces and moments

	R_X	M_Z	$\Delta F_{SZ}+\Delta P_{in}A_{inZ}$	M_{WJ}
CFD-WJM	-8.767×10^{-5}	2.755×10^{-5}	-6.35×10^{-5}	1.597×10^{-5}

as $E(\%D)=(\text{EFD}-\text{CFD})/\text{EFD}\times100$. The error in sinkage is $E=0.8\%$, and the trim is 14.3%. The errors are within the range of error values obtained from this code in previous simulations (Table 1). For the towed propelled simulations, the errors for resistance, sinkage, and trim are −4.6%, 9.0%, and 13.6%, respectively.

Waterjet induced changes in sinkage and trim were estimated using hydrostatic approximations [11]. The hydrostatic heave restoring force is written as the incremental heave for an incremental restoring force,

$$\Delta\sigma = R_Z/\rho g A_{WP} \tag{24}$$

where $\Delta\sigma$ is the induced sinkage due to the waterjet, ρ is the density of water, and $A_{WP}=0.0509L_0^2=2.4631$ m^2 is the water plane area [10]. The standard moment to trim 1 deg was modified to account for any small incremental angle instead of 1 deg. This results in the following expression:

$$\Delta\tau \approx \sin^{-1}(M_{WJ}/\rho g I_L) \tag{25}$$

where $\Delta\tau$ is the waterjet induced change in trim angle and I_L is the longitudinal moment of inertia about the center of flotation. The results are summarized in Table 7.

Table 7 includes CFD predictions of waterjet induced sinkage and trim. The E=−58%D and 11.5%D for $\Delta\sigma$ and $\Delta\tau$ are larger than the hydrostatic estimates. Table 7 also shows the relative induced change in sinkage $\Delta\sigma/\sigma_{BH}$ and trim $\Delta\tau/\tau_{BH}$, which serves as a better measure of the waterjet/hull interaction than $\Delta\sigma$ and $\Delta\tau$. The towed bare hull CFD simulation values of sinkage σ_{BH} and trim τ_{BH} are used in the computation of $\Delta\sigma/\sigma_{BH}$ and $\Delta\tau/\tau_{BH}$ for the CFD predictions. The CFD waterjet model underpredicts $\Delta\sigma/\sigma_{BH}$ as $\Delta\sigma/\sigma_{BH}=7.01\%$ compared to the EFD value of 16.97%; for $\Delta\tau/\tau_{BH}$, the CFD waterjet model predictions are reasonable as $\Delta\tau/\tau_{BH}=25.51\%$ compared to $\Delta\tau/\tau_{BH}=24.57\%$ reported by EFD.

The large relative induced change in sinkage and trim show that the waterjet/hull interaction is significant. However, because the absolute magnitudes of the induced sinkage and trim are small, the change in resistance between the towed bare hull and towed propelled models at the same speed is small. This result indicates that for this displacement ship at this Froude number the change in sinkage and trim due to the waterjet/hull interaction will not affect speed significantly for the same power.

5.3 Validation of Local Variables. The primary purpose of implementing the waterjet model using waterjet model input data from experiments is that flow details such as boundary layer profiles, bow/sonar-dome vortices, and wave elevations, which are expensive to obtain from experiments, can be obtained through the simulations. This is especially true when far-field wave elevation is required, which in some cases is highly sensitive to waterjet induced changes in trim angle. Wave elevation data are unavailable for the 5594 self-propelled cases. Here, the predictive capability of CFDShip for local flow variables is demonstrated in Fig. 6, which shows the nominal wake contours of the nondimensional axial velocity immediately upstream of the waterjet inlet ($x/L=0.93$), with the inlets closed and the model towed at a fixed sinkage and trim condition equal to that of the self-propelled case. The CFD contours show a good agreement with the EFD [9], with a slight overprediction of the boundary layer thickness.

6 Correlations for CFD Waterjet Model

Ultimately, the waterjet model will be of most use if general correlations can be obtained, which would provide the waterjet flow input variables. Recently, detailed self-propulsion simulation of waterjet appended ships has been performed, which provides opportunity to investigate if such correlations are feasible. Kandasamy et al. [4] provided detailed self-propulsion simulation results for waterjet appended JHSS. The results were validated using experimental data [12]. In addition, simulation results are also available for Delft catamaran (DC) for which experimental results for validation are available from the ongoing ONR collaborative

Table 6 Results of predicted total resistance, sinkage, and trim for the towed and self-propelled simulations

Cases		C_{TX}	$-R_X+F_D$	E (%D)	σ (z/L_0)	E (%D)	τ (rad)	E (%D)
Towed, bare hull	EFD	1.4288×10^{-4}	–	–	-1.438×10^{-3}	–	6.35×10^{-3}	–
	CFD	1.4176×10^{-4}	–	+0.78	-1.427×10^{-3}	+0.8	5.44×10^{-3}	+14.3
Towed, propelled	EFD	–	1.3870×10^{-4}	–	-1.682×10^{-3}	–	7.91×10^{-3}	–
	CFD-WJM	1.4507×10^{-4}	–	−4.6	-1.527×10^{-3}	+9.0	6.82×10^{-3}	+13.7

Table 7 Waterjet induced sinkage $\Delta\sigma$ and trim $\Delta\tau$

	Waterjet induced sinkage and trim						
Cases	$\Delta\sigma$ (z/L)	$\Delta\sigma$/draft %	E (%D)	$\Delta\sigma/\sigma_{BH}$%	$\Delta\tau$ (rad)	E (%D)	$\Delta\tau/\tau_{BH}$ %
EFD	-2.44×10^{-4}	0.90	–	16.97	1.56×10^{-3}	–	+24.57
Hydrostatic Est.	-1.84×10^{-4}	0.70	−22.2	13.10	1.562×10^{-3}	−1.3	+24.60
CFD-WJ model Predictions	-1×10^{-4}	0.37	−58.9	7.01	1.38×10^{-3}	+11.5	+25.51

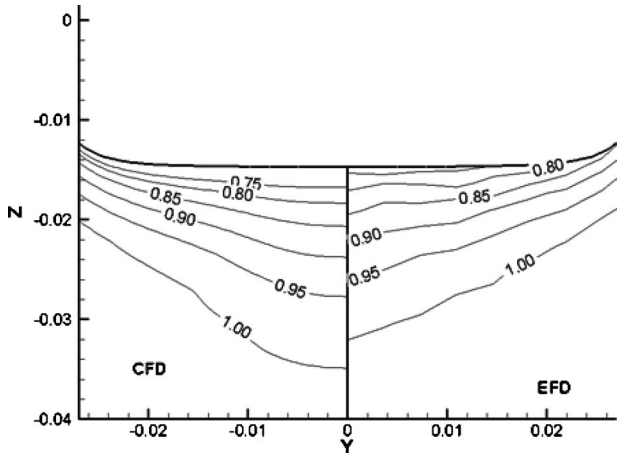

Fig. 6 Contours of bare hull axial velocity upstream of the waterjet inlets at $X/L=0.96$

project with the Bulgarian Ship Hydrodynamics Centre [13]. In this section, we explore the possibility of obtaining suitable correlations from self-propulsion simulations for JHSS and DC, along with the experimental data available for 5594.

Figure 7(*a*) shows the bare hull resistance C_{TX} and the self-propelled net jet thrust R_X for both the experiments and the simulations. Detailed waterjet self-propelled simulation results are available in the range $0.18<\mathrm{Fr}<0.39$ for JHSS and $0.46<\mathrm{Fr}<0.80$ for DC, along with validation data. Bare hull validation data are available for DC over a wider range $0.20<\mathrm{Fr}<0.70$. R_X is available for 5594 only at Fr=0.511, and C_{TX} is available over the whole range $0.20<\mathrm{Fr}<0.80$. From the simulation results, R_X for JHSS and DC was obtained using the CFD waterjet model control volume and is within ±2% of the values obtained using the ITTC control volume. A log scale is used in the plots since C_{TX} and R_X values for DC are up to an order of magnitude higher than JHSS and 5594 for the following reasons: (1) The nondimensionalization parameter is L^2, and being a catamaran in addition to having a lower demihull slenderness ratio than the other two hulls, the wetted surface area to L^2 ratio for DC is almost four times larger than JHSS and 5594, and (2) the values for DC are at the model scale, whereas JHSS and 5594 were investigated with a full-scale thrust identity and added tow force. In Fig. 7(*a*), the added tow force has been subtracted from the bare hull C_{TX} for JHSS and 5594 to enable a comparison with R_X and for the calculation of the thrust deduction fraction t.

For DC, C_{TX} and R_X are within 3.9% and 9% of the benchmark data, respectively. For JHSS, C_{TX} and R_X are within 6.2% and 7.1% of the data, respectively. Both DC and 5594 show the characteristic C_{TX} hump at $\mathrm{Fr}\sim0.5$, but it is more prominent for DC. Data are not available for JHSS at the hump region. The simulations show a reasonably good agreement with data for the thrust deduction fraction t (Fig. 7(*b*)). The experiments show a negative thrust deduction for 5594 at Fr=0.51; simulations are not available for this condition. Figure 7(*c*) shows the sinkage for the different hulls. For both DC and JHSS, simulations and experiments show negligible effect of the waterjet on the sinkage, and the simulation results correspond well with the data. The waterjet induced increase in trim (Fig. 7(*d*)) is highest for DC, moderate for 5594, and comparatively negligible for JHSS. The simulation and experimental trim values compare well for both DC and JHSS.

The transom vertical force components for the different hulls over the Fr range shown in Fig. 8(*a*) show similar trends as R_X in Fig. 7(*a*). DC vertical forces are almost an order of magnitude greater than JHSS and 5594, and the peak is at $\mathrm{Fr}\sim0.5$, similar to R_X. For JHSS, both the vertical forces and R_X indicate a gradual rise after Fr=0.3. The inlet velocity ratio (IVR), which is $\bar{V}_{A\mathrm{in}}$ from Eq. (2) normalized by the freestream velocity U_0, is plotted alongside and also shows similar trends as the vertical force components. Plotting the vertical forces against the IVR (Fig. 8(*b*))

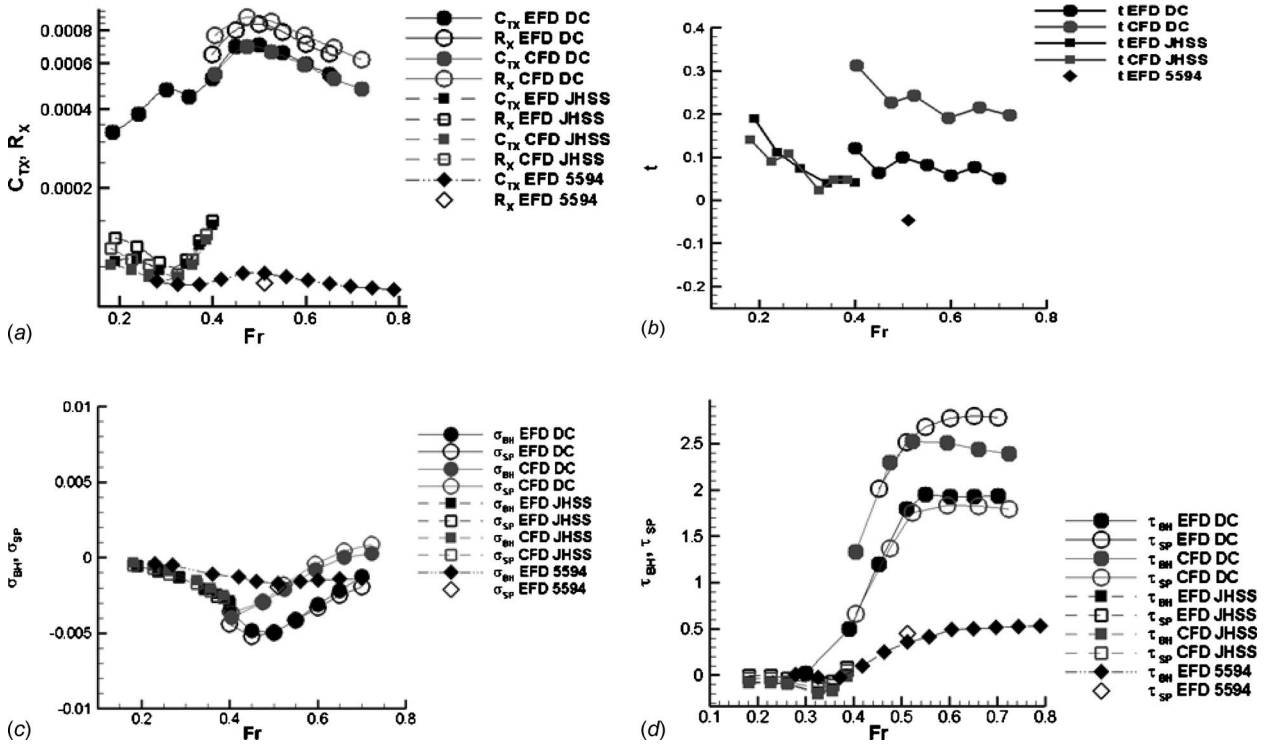

Fig. 7 Forces and motions: (*a*) bare hull C_{TX} and self-propelled R_X for three different hull forms, (*b*) thrust deduction, (*c*) sinkage, and (*d*) trim

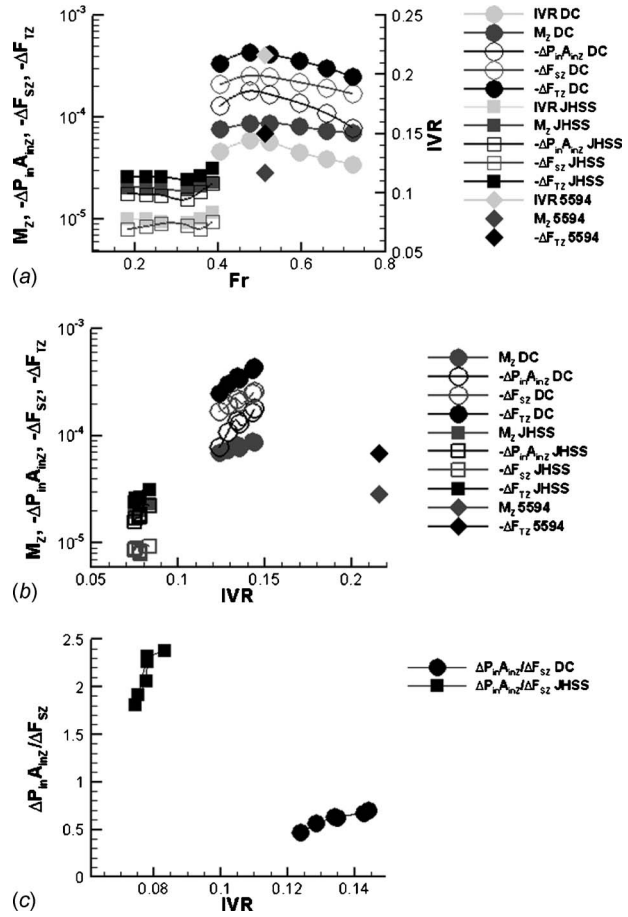

Fig. 8 Vertical forces: (*a*) vertical forces versus Fr, (*b*) vertical forces versus IVR, and (*c*) vertical force component ratio variation with IVR

indicates a noticeable log-linear trend between the vertical forces and IVR for both JHSS and DC. Since the vertical forces for DC is about an order of magnitude greater than the other two hulls, a generalized correlation between the vertical force components and the IVR that can encompass all the hulls is unattainable. Figure 8(*c*) shows the relative contributions of $\Delta P_{\text{in}}A_{\text{in}Z}$ and ΔF_{SZ} by plotting the ratio $\Delta P_{\text{in}}A_{\text{in}Z}/\Delta F_{SZ}$ against IVR. The differences in the waterjet inlet and hull designs account for the dominance of the $\Delta P_{\text{in}}A_{\text{in}Z}$ component in JHSS and the ΔF_{SZ} component in DC. For both hulls, the contribution of $\Delta P_{\text{in}}A_{\text{in}Z}$ component increases with increasing IVR.

Figures 9(*a*) and 9(*b*) give the variation in ϕ and ϕ/ϕ' versus IVR, respectively. A linear least squares fit (LSF) over the data for ϕ over all the points is possible with a correlation coefficient (R^2) of 0.98. The variation in ϕ/ϕ' is small, between 0.5 and 0.6, for the different ships over the IVR range, and a linear LSF gives $R^2=0.82$. Figure 10 shows the momentum correction factors of the waterjet inlet versus IVR. A LSF with a second order polynomial gives R^2 values of 0.98 for both C_{MinX} and C_{MinZ}. C_{M6} at the outlet is almost constant $\sim 1.03 \pm 2\%$.

Noting that both C_{TX} and $-F_{TZ}$ for DC are almost an order of magnitude higher than the other two hulls, a general correlation for the vertical forces to encompasses all the different hull/waterjet designs seems possible by plotting the ratio $-F_{TZ}/C_{TX}$ against IVR (Fig. 11). This ratio is similar to the lift/drag coefficients used in aerospace engineering. C_{TX} is used here instead of R_X since R_X will be unavailable during the implementation of the waterjet model for predictive purposes. A logarithmic LSF fit over all the hulls is possible with $R^2=0.95$. Note that $\Delta P_{\text{in}}A_{\text{in}Z}$ for 5594

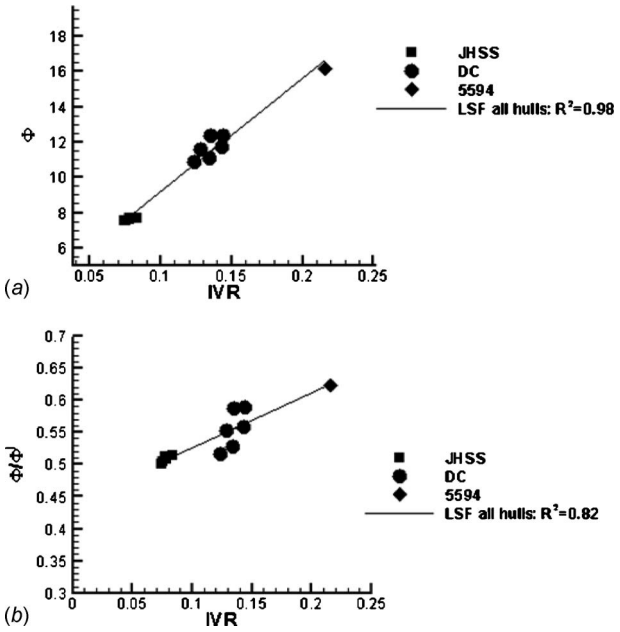

Fig. 9 Inlet flow angles: (*a*) Φ *versus IVR (b)* Φ/Φ' *versus IVR*

was approximated by the closest pressure measurements at the stern and is not an accurate representation of its true value, as evident from Fig. 8(*c*). A logarithmic LSF fit with $R^2=0.98$ is possible if only JHSS and DC are considered.

These correlations provide all the waterjet inlet flow variables as a function of IVR. Equation (10) can be rewritten as functions of IVR as follows:

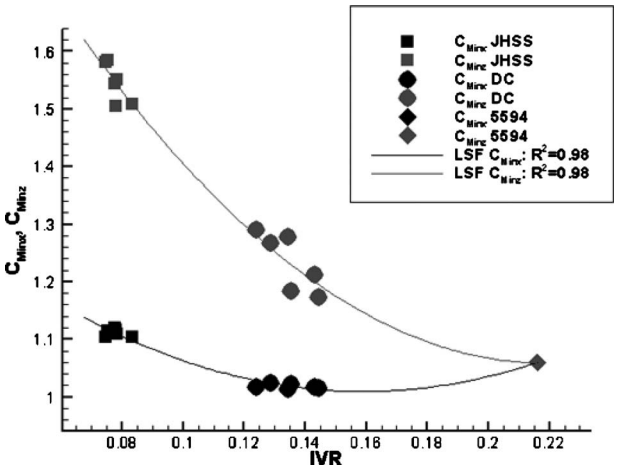

Fig. 10 Momentum correction factors at A_{in}

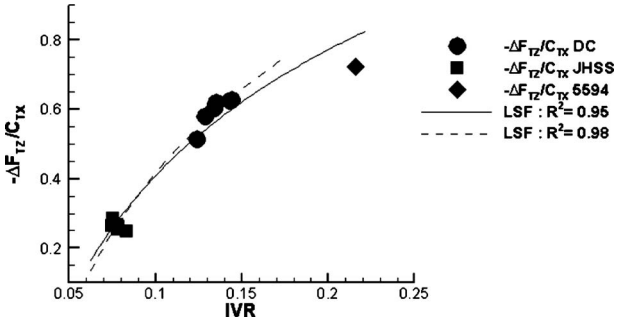

Fig. 11 Correlation of vertical force coefficients

$$R_X = fn(\mathrm{IVR}) = -\mathrm{IVR}^2 \times A_{\mathrm{in}Z}\left(c_{M6}\frac{A_{\mathrm{in}Z}}{A_{6X}} - c_{M\mathrm{in}X}\cot\phi\right) \quad (26)$$

As an initial guess, the waterjet geometric angle information can be used to get an estimate of the inflow angle assuming inflow/geometric angle ratio ~ 0.55. The corresponding IVR is obtained from Fig. 9(*b*). For a particular Fr, based on C_{TX} and the initial IVR estimates, the total vertical stern force is calculated using the correlation from Fig. 11, which provides ΔF_{TZ}, and the vertical momentum flux term is obtained as

$$M_Z = \mathrm{IVR}^2 \times A_{\mathrm{in}Z} \times c_{M\mathrm{in}Z} \quad (27)$$

A towed propelled simulation can be conducted at the particular Fr to obtain a new R_X. IVR is then recalculated from Eq. (26). $c_{M\mathrm{in}Z}$ is recalculated for the new IVR, and M_Z is obtained from Eq. (27). The vertical forces are recalculated based on the new IVR from Fig. 11, and the steps are iterated until convergence.

7 Conclusions

An integral force/moment waterjet model for CFD is derived for ship local flow/powering predictions, including sinkage and trim. The CFD waterjet model is derived in a ship-fixed reference frame and extends the ITTC waterjet model by using a control volume appropriate for CFD, which includes vertical forces R_Z and angular momentum M_{RY}. In addition, the model accounts for the waterjet-hull interaction by incorporating a stern force $\Delta\mathbf{F}_S$ in the balance of forces and moments for the ship. This allows the CFD waterjet model to predict sinkage and trim in addition to resistance for waterjet-propelled ships without requiring detailed modeling of the waterjet geometry.

The model is demonstrated and validated using existing data from towing tank experiments of a towed bare hull and towed propelled DTMB 5594 using R_X from EFD as an input parameter to estimate ϕ, which was not measured. The effects of the model on sinkage and trim are qualitatively examined using hydrostatics. The hydrostatic estimates show good agreement with experimental data. The model is then implemented in a CFD code, CFDSHIP-IOWA 4.0. A baseline CFD simulation is carried out, mimicking the towed bare hull condition, showing good quantitative agreement with EFD results especially with regard to resistance, $E=0.78\%$, and sinkage, $E=0.8\%$, and reasonably good agreement for trim, $E=14.3\%$. The CFD waterjet model is shown to be reasonably accurate in predicting resistance, $E<5\%$, sinkage, $E=9.0\%$, and trim, $E=13.7\%$, as the errors are comparable in magnitude to previous simulations using the code. However, the thrust deduction fraction t from the simulations is positive, whereas the data indicate negative t. Such application of the model will be useful for the prediction of local flow variables, which are difficult to measure in experiments. The ITTC procedures, which already require extensive data collection, could be extended to measure the input variables required for the CFD waterjet model. Pressure measurements at the inlet would allow for separately specifying $\Delta P_{\mathrm{in}}\mathbf{A}_{\mathrm{in}}$ and $\Delta\mathbf{F}_S$, instead of approximating $\Delta P_{\mathrm{in}}\mathbf{A}_{\mathrm{in}}$ using the pressure at the vicinity of the inlet, as was done for the current validation.

The model can also be used for powering predictions once waterjet flow input variable correlations are available based on CFD for the waterjet system and/or experimental data. Detailed waterjet flow simulation results from JHSS and DC were used along with available data for DTMB 5594 to derive correlations for the waterjet model input variables. Correlations obtained from this limited analysis indicate that this approach is feasible. However, additional detailed simulations and experiments for different waterjet/hull geometries over a wide range of operating conditions need to be investigated before such correlations can be fully established.

Acknowledgment

This research is sponsored by Pacific International Engineering PLLC (Contract No. KT-05-343) under the administration of Dr. Philip D. Osborne and by the Office of Naval Research (Grant No. N00014-08-1-0491) under the administration of Dr. Ki-Han Kim.

References

[1] Van Terwisga, T., 2005, "Report of the Specialist Committee on Validation of Waterjet Test Procedures," Proceedings of the 24th International Towing Tank Conference, Vol. II, pp. 471–508.
[2] Stern, F., Carrica, P., Kandasamy, M., Gorski, J., O'Dea, J., Hughes, M., Miller, R., Kring, D., Milewski, W., Hoffman, R., and Cary, C., 2007, "Computational Hydrodynamic Tools for High-Speed Sealift," Transactions of The Society of Naval Architects and Marine Engineers, **114**, pp. 55–81.
[3] Carrica, P. M., Wilson, R. V., and Stern, F., 2007, "An Unsteady Single-Phase Level Set Method for Viscous Free Surface Flows," Int. J. Numer. Methods Fluids, **53**, pp. 229–256.
[4] Kandasamy, M., Takai, T., and Stern, F., 2009, "Validation of Detailed Waterjet Simulation Using URANS for Large High-Speed Sea-Lifts," Tenth International Conference on Fast Sea Transportation, Athens, Greece.
[5] Stern, F., Kim, H. T., Zhang, D. H., Toda, Y., Kerwin, J., and Jessup, S., 1994, "Computation of Viscous Flow Around Propeller-Body Configurations: Series 60 CB=6 Ship Model," J. Ship Res., **38**(2), pp. 137–157.
[6] Kandasamy, M., Ooi, S. K., Carrica, P., Stern, F., Campana, E., Peri, D., Osborne, P., Cote, J., Macdonald, N., and Waal, N. D., 2009, "URANS Based Optimization of a High-Speed Foil-Assisted Semi-Planning Catamaran for Low Wake," Tenth International Conference on Fast Sea Transportation, Athens, Greece.
[7] Carrica, P. M., Wilson, R. V., Noack, R. W., and Stern, F., 2007, "Ship Motions Using Single-Phase Level Set With Dynamic Overset Grids," Comput. Fluids, **36**, pp. 1415–1433.
[8] Xing, T., Carrica, P., and Stern, F., 2008, "Computational Towing Tank Procedures for Single Run Curves of Resistance and Propulsion," ASME J. Fluids Eng., **130**(2), pp. 1–14.
[9] Wilson, M. B., Gowing, S., Chesnakas, C., and Lin, C. W., 2005, "Waterjet-Hull Interactions for Sealift Ships," International Conference on Marine Research and Transportation (ICMRT'05), Italy.
[10] Miller, R., 2007, private communication.
[11] 1988, *Principles of Naval Architecture*, E. V. Lewis, ed., SNAME, New York, Vol. I.
[12] Jessup, S., Donnelly, M., Fry, D., Cusanelli, D., and Wilson, M., 2008, "Performance Analysis of a Four Waterjet Propulsion System for a Large Sealift Ship," 27th Symposium on Naval Hydrodynamics, Seoul, Korea.
[13] Georgiev, R., 2010, "Model Tests of Waterjet Propelled Delft 372 Catamaran," Technical Report No. KP 092006/01.